LARGE EDDY SIMULATIONS OF ROTATING SQUARE DUCT WITH NORMAL RIB TURBULATORS

MAYANK TYAGI, ARUN K. SAHA, SUMANTA ACHARYA
Mechanical Engineering Department
Louisiana State University, Baton Rouge, LA

Abstract

Large Eddy Simulations (LES) were performed to study the flow physics and heat transfer in a rotating ribbed duct. This numerical study is simulating the experiments conducted to investigate the effects of buoyancy and Coriolis forces on heat transfer in a turbine blade internal coolant passages (Wagner et al., 1992). The computations were performed at a Reynolds number (*Re*) of 12,500 based on average velocity in the duct and the hydraulic diameter of the square duct. The rotation number (*Ro*) is 0.12 and the inlet coolant-to-wall density ratio ($\Delta\rho/\rho$) is 0.13. The rib height-to-hydraulic diameter ratio (*e/D*) is 0.1 and the rib pitch-to-height ratio (*P/e*) is 10. The ribs are square in cross-section and are placed transverse to the flow in the duct. A direct method of computing a source term due to unsteady calculation of uniform wall temperature case in periodic geometries is presented. The details of flow field and the temperature field are presented and analyzed.

1. Introduction

Modern gas turbines operate at very high turbine inlet temperatures for better second law efficiency and specific thrust. However, such increased thermal loads can deteriorate the blade life in a rotating environment. These blades are internally cooled by using the serpentine channels with turbulators inside the blade to enhance the heat transfer (Morris, 1981). The increment in heat transfer due to rib turbulators as compared to the increased pressure drop in the channel is a crucial design parameter. The problem is complicated further due to the interplay of Coriolis forces and buoyancy forces. Several experimental investigations to study the effect of centrifugal buoyancy, rotation number and Reynolds number have been performed (Wagner et al., 1992). However, a numerical study can provide much more detailed information on flow physics as well as heat transfer in such situations. The secondary flow in non-circular duct without rotation is generated due to the anisotropy in turbulent stresses. In rotating ducts, the Coriolis forces give rise to secondary flow as well. Again, buoyancy forces can generate secondary flow field to enhance the crossplane mixing. Low-level turbulence modeling using two-equation models is incapable of capturing essential physics due to isotropic nature of modeled turbulent stresses (Hermanson et al., 2001). Second moment closure has some promise in that direction (Jang et al., 2001). To understand the unsteady dynamics of various flow structures on the heat transfer, it is inevitable to use LES (Murata et al., 2000 and 2001).

2. Governing Equations

The non-dimensional governing equations for conservation of mass, momentum and energy for an incompressible Newtonian fluid in LES methodology are as follows

$$\frac{\partial U_j}{\partial x_j}=0$$

$$\frac{\partial U_i}{\partial t}+\frac{\partial U_i U_j}{\partial x_j}=-\frac{\partial p}{\partial x_i}-\frac{dP}{dz}\delta_{i3}+\frac{1}{\mathrm{Re}}\frac{\partial^2 U_i}{\partial x_j^2}+\frac{\partial \tau_{ij}}{\partial x_j}-2Ro\varepsilon_{ijk}\Omega_j U_k+Bo\left(1-\frac{\Theta}{\Theta_b^0}\right)\left(\varepsilon_{ijk}\varepsilon_{klm}\Omega_j\Omega_l r_m\right)$$

$$\frac{\partial \Theta}{\partial t}+\lambda\Theta+U_j\frac{\partial \Theta}{\partial x_j}=\frac{1}{\mathrm{Re}\,\mathrm{Pr}}\frac{\partial^2\Theta}{\partial x_j^2}+\frac{\partial q_j}{\partial x_j}$$

where U_i is the filtered velocity field, $\Theta=\frac{T-T_1}{T_w-T_2}$ where T_w is the wall temperature and T_1 , T_2 are yet undefined reference temperatures. The mean pressure gradient in flow direction is dP/dz. Therefore, p is the periodic component of the pressure field. δ_{ij} is the Kronecker delta tensor. ε_{ijk} is the alternating tensor. The distance vector can be written as $r_i=R_m\delta_{i3}+x_i$, where R_m is the mean radius of the periodic module from the rotation axis. The important parameters for such flows are Reynolds number ($Re=U_m D_h/\nu$), rotation number ($Ro=\Omega\left(D_h/U_m\right)$) and centrifugal buoyancy number ($Bo=\frac{\beta(T-T_{in})\Omega^2 R_m D_h^3}{\nu\alpha}=\left(\frac{\alpha}{\nu}\right)\left(\frac{D_h/U_m}{1/\Omega}\right)^2=\frac{Ra_\Omega}{\mathrm{Pr}\,\mathrm{Re}^2}$). The SubGrid Scale (SGS) stress tensor and SGS scalar flux vector are given by τ_{ij} and q_j respectively. In this study, Dynamic Mixed Model (DMM) is used to model these SGS stress tensor and scalar flux vector (Moin et al., 1991, Vreman et al., 1994). The box filters are used in the Germano identity for the calculation of dynamic coefficient and for the calculation of Leonard stresses. The dynamic coefficient is test filtered to avoid numerical instabilities. Treatment of the non-dimensional temperature in the periodic direction needs special attention. Patankar et al. (1977) described a method to solve the uniform heat flux (UHF) and uniform wall temperature (UHT) problems in the ducts with periodic cross-sections for steady situations. Wang and Vanka (1989) presented an iterative procedure to calculate λ. However, this parameter can be calculated directly for explicit schemes. Most of the simulations were performed using non-dimensionalization with respect to friction velocity and uniform heat flux case. As it will be explained later, that renders the sink terms in momentum and energy equations, i.e. dP/dz and λ, constant. In experiments, usually the mass flow rate and wall temperatures are control parameters, therefore reference velocity should be the average velocity and λ is no more constant.

Boundary conditions for non-dimensional temperature in the periodic direction is written as

$$\frac{\Theta^0}{\Theta_b^0}=\frac{\Theta^L}{\Theta_b^L}$$

where superscript indicates the z-location and subscript *b* denotes the bulk non-dimensional temperature. Differentiating the periodic boundary condition in the wall-normal direction we get

$$\frac{1}{\Theta_b^0}\left(\frac{\partial\Theta^0}{\partial X}\right)=\frac{1}{\Theta_b^L}\left(\frac{\partial\Theta^L}{\partial X}\right)$$

This is equivalent to enforcing periodicity on the Nusselt number in a periodic geometry.

Uniform Heat Flux (UHF) case:

$$\left(\frac{\partial\Theta^0}{\partial\eta}\right)=\left(\frac{\partial\Theta^L}{\partial\eta}\right)=q_w$$

$$\therefore \Theta_b^0=\Theta_b^L$$

Clearly, setting T_2 to T_b will render the denominator as a constant. Moreover, the independence of non-dimensional bulk temperature from periodic direction implies that T_1 is equal to T_b. Therefore, the scaling at the inlet plane and periodicity of Nusselt number can uniquely determine the non-dimensionalization and the sink term in the energy equation.

Uniform Wall Temperature (UWT) case:

From the energy balance, one can write

$$\rho C_p U_{avg}\left(T_b^L-T_b^0\right)A_c=\iint_S q_w dS$$

$$\iint_S q_w dS\approx\sum_{in} q_w dS+\sum\left(q_w^0+q_w^L\right)\frac{dS}{2}$$

$$\rho C_p U_{avg}\left(T_w-T_2\right)\left(\Theta_b^L-\Theta_b^0\right)A_c\approx k\left(T_w-T_2\right)H\left[\sum_{in}\left(\frac{\partial\Theta}{\partial\eta}\right)_w dS+\sum\left(\left(\frac{\partial\Theta}{\partial\eta}\right)_w^0+\left(\frac{\partial\Theta}{\partial\eta}\right)_w^L\right)\frac{dS}{2}\right]$$

Here η is the wall normal direction and dS is the differential area element on the wall.

For the square channel, we use Nusselt number periodicity to define the flux at the inlet in terms of the flux at the exit as

$$\left(\frac{\partial\Theta}{\partial\eta}\right)_w^0=\frac{\Theta_b^0}{\Theta_b^L}\left(\frac{\partial\Theta}{\partial\eta}\right)_w^L$$

$$\lambda\equiv\frac{\Theta_b^0}{\Theta_b^L}$$

Using these relations in the energy balance, we get

$$\left(\Theta_b^L - \lambda\Theta_b^L\right)A_c \approx \left(\frac{1}{\mathrm{Re}\cdot\mathrm{Pr}}\right)\left[\sum_{in}\left(\frac{\partial\Theta}{\partial\eta}\right)_w dS + \sum\left(\lambda\left(\frac{\partial\Theta}{\partial\eta}\right)_w^L + \left(\frac{\partial\Theta}{\partial\eta}\right)_w^L\right)\frac{dS}{2}\right]$$

$$\therefore \lambda \approx \frac{\left\{\Theta_b^L - \left(\frac{1}{\mathrm{Re}\cdot\mathrm{Pr}}\right)\left[\sum_{in}\left(\frac{\partial\Theta}{\partial\eta}\right)_w dS + \sum\left(\frac{\partial\Theta}{\partial\eta}\right)_w^L \frac{dS}{2}\right]\right\}}{\left\{\Theta_b^L + \left(\frac{1}{\mathrm{Re}\cdot\mathrm{Pr}}\right)\left[\sum\left(\frac{\partial\Theta}{\partial\eta}\right)_w^L \frac{dS}{2}\right]\right\}}$$

To enforce the validity of scaling relation up to the wall, we choose T_1 equal to T_w. Therefore, the non-dimensional temperature is zero at the wall and the scaling ensures the periodicity of the Nusselt number in the periodic geometries.

3. Problem Description and Computational Method

The computations were performed at a Reynolds number (*Re*) of 12,500 based on average velocity in the duct and the hydraulic diameter of the square duct. The rotation number (*Ro*) is 0.12 and the inlet coolant-to-wall density ratio ($\Delta\rho/\rho$) is 0.13. The rib height-to-hydraulic diameter ratio (*e/D*) is 0.1 and the rib pitch-to-height ratio (*P/e*) is 10. The ribs are square in cross-section and are placed transverse to the flow in the duct. This numerical study is simulating the experiments conducted to study the effects of buoyancy and Coriolis forces on heat transfer in turbine blade internal coolant passages (Wagner et al., 1992).

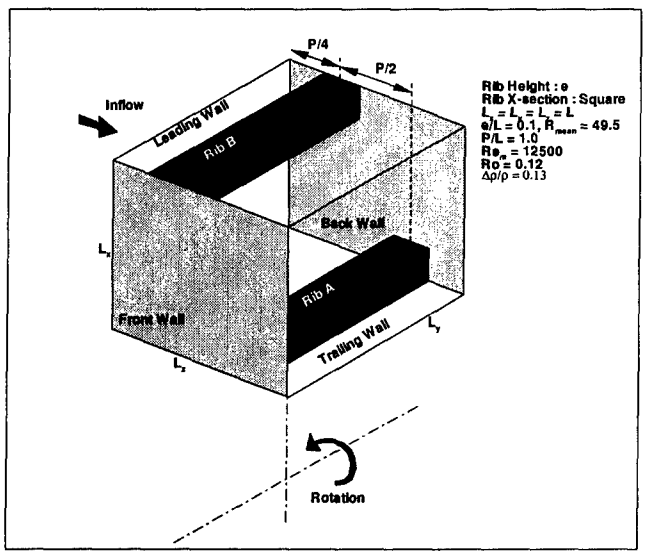

Figure 1 Schematic of the computational domain

4. Results and Discussion

The three-dimensional spectrum of the instantaneous flow field is shown in figure 2a. The grid resolution is sufficient to capture the energy producing

events as well as the portion of the inertial subrange. A peak in energy spectrum is also observed around the wave number corresponding to a length scale l/D = 0.16. Clearly, this can be attributed to the energy production by vortex shedding behind the ribs (e/D = 0.1). To maintain the flow rate, the mean pressure gradient is applied. However, this pressure gradient is subjected to temporal variations corresponding to the Strouhal frequency of vortex shedding due to ribs. This pulsation causes the flow rate to vary with the same frequency (figure 2b). The average flow rate is maintained at 1.0 as desired.

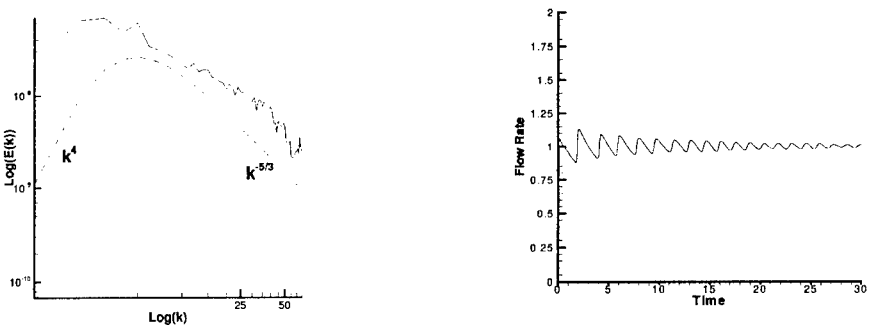

(a) (b)

Figure 2 (a) Three dimensional energy spectrum of the flow field (b) Flow rate vs time.

FLOW FIELD DESCRIPTION

The instantaneous snapshots of the streamwise component of vorticity field at three different streamwise stations (z/D = 0.25, 0.50 and 0.75) depict the complex flow field in the duct (figure 3). At z/D = 0.25, the rib is placed on the leading wall and sheds vortices into the mainflow with significant streamwise vorticity. The boundary layer on the trailing wall is highly turbulent and intensified. The local increase in velocity magnitude near the trailing wall is due to decrease in cross-sectional area as well as body forces. At the streamwise centerplane z/D = 0.50, the recirculation region behind the rib on the leading wall contains intense vortices along the flow. The trailing wall vortices are gathered towards the center of the duct due to secondary flow in the crossplane of the duct. At z/D = 0.75, the rib is placed on the trailing wall and interacts with the oncoming turbulent boundary layer vortices. In this snapshot, the vortices are pushed towards the center of duct by the rib as well as the secondary flow. The leading wall boundary layer shows a lot of activity too. The vortices at the front and the back wall do not penetrate into the core flow to the similar extent as the leading and trailing wall vortices.

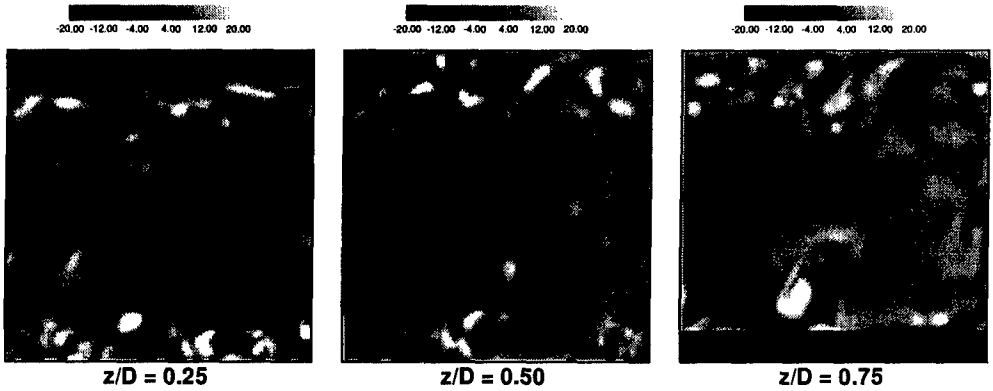

Figure 3 Streamwise component of instantaneous vorticity ω_z at three XY planes

Time-averaged velocity field shows the skewed profile (Figure 4). The boundary layer on the trailing wall (unstable) is much steeper than on the leading wall (stable). The details near the ribs show the difference in the size of recirculation regions in front and behind the ribs. The flow attaches over the top of the rib B (on the trailing wall) while it remains detached on the top face of rib A (on the leading edge). The impingement of the oncoming flow on the front of the ribs results in high heat transfer rates. The recirculation behind the ribs accompanied with enhanced crossplane mixing will result in the increased heat transfer rates.

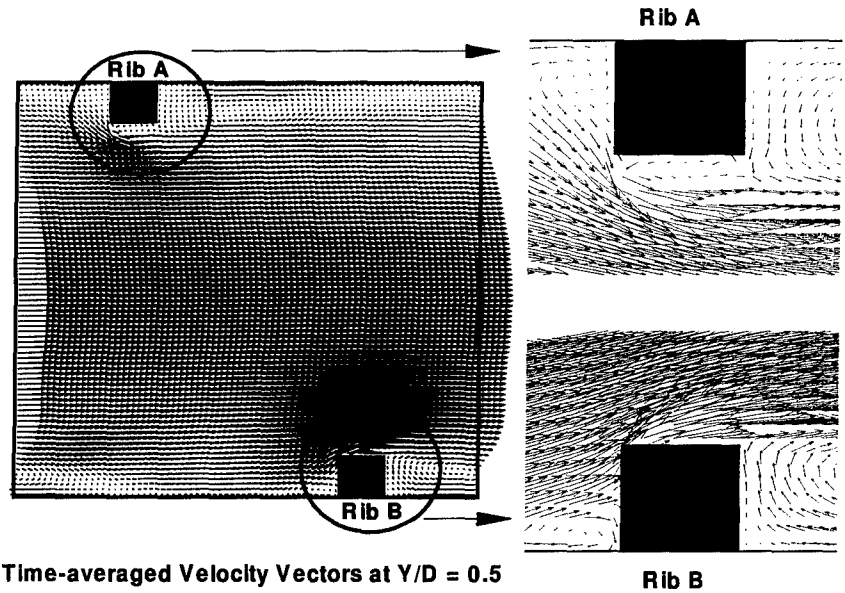

Figure 4 Time-averaged velocity vectors and details of flow field near the ribs at the Y/D = 0.5

HEAT TRANSFER RESULTS

Instantaneous non-dimensional temperature field is shown at the first cell node over the corresponding walls. There is more coolant accumulation on the trailing wall as compared to the leading wall (note the difference in the range). The heat transfer is enhanced on the trailing wall by a factor of two approximately. The temperature field show streaks correlated with the streamwise component of vorticity on these walls. The coolant fluid in front of the ribs increases heat transfer in the stagnation (front recirculation) region. In the leeward recirculation regions, the non-dimensional temperature is close to wall temperature. The temperature distribution on the front and back wall is similar. However, there is more coolant near the back wall as compared to front wall (and it is observed through out the computational duration). This might be caused by a low frequency mode in the coreflow. Again, the temperature field correlates with the streamwise streaks of coolant fluid on these walls.

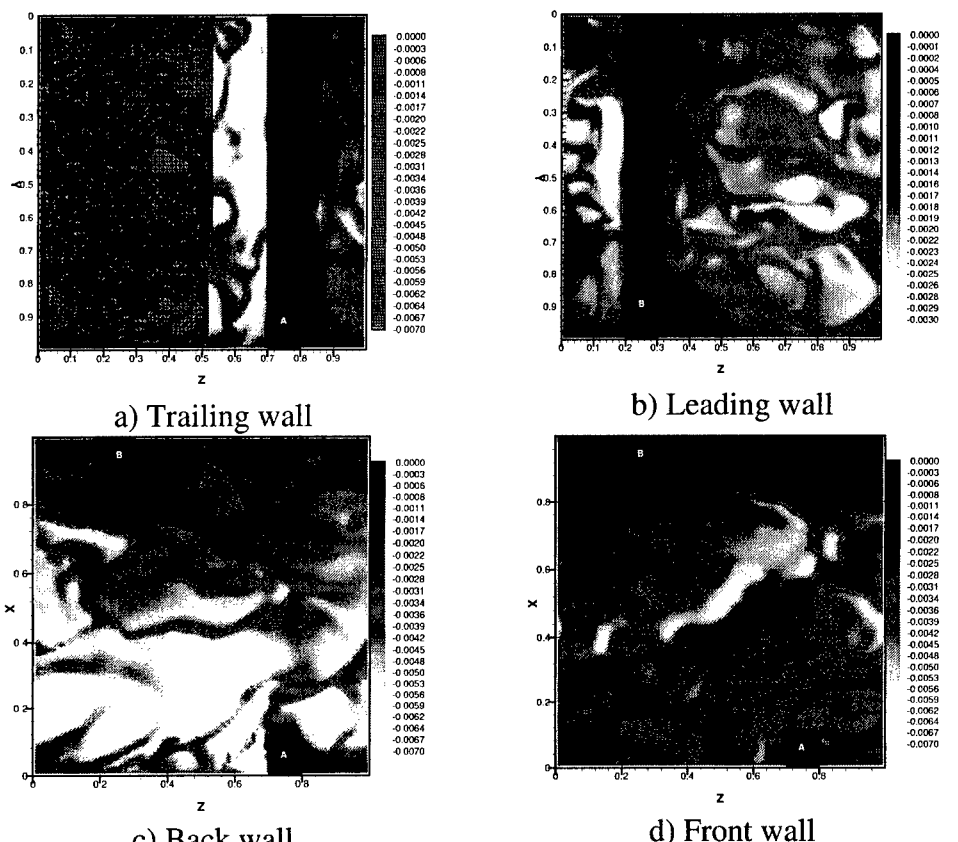

Figure 5 Instantaneous temperature field on the walls of the duct a) Trailing wall, b) Leading wall, c) Back wall and d) Front wall.

5. Conclusion

Large eddy simulations were performed for a rotating square duct with normal rib turbulators to enhance the heat transfer. The Coriolis force as well as

centrifugal buoyancy parameter has been included in this study. A direct approach is presented for the unsteady calculation of non-dimensional temperature field in periodic domains. The complex flow field shows dominant secondary flow vortices that enhance the mixing of the thermal boundary layers on the duct walls with the coolant fluid in the core. The temperature field is highly unsteady and may contain low frequency mode that allows the coolant to adhere to either front or the back wall of the duct. In the future, the assessment of heat transfer enhancement with respect to increased pressure loss will be presented.

References

Chen, Y., Nikitopoulos, D.E., Hibbs, R., Acharya, S. and Myrum, T.A. (2000) Detailed mass transfer distribution in a ribbed coolant passage with a 180° bend, *Int. J. Heat Mass Transfer*, Vol. 43, pp. 1479-1492.

Hermanson, K., Parneix, S. and Von Wolfersdorf, J. (2001), Prediction of pressure loss and heat transfer in internal cooling passages with rotation (*Preprint*).

Jang, Y.-J., Chen, H.-C. and Han, J.-C. (2001) Flow and heat transfer in a rotating square channel with 45° angled ribs by Reynolds stress turbulence model, *J. Turbomachinery*, Vol. 123, pp.124-132.

Moin, P., Squires, K., Cabot, W. and Lee, S. (1991), A dynamic subgrid-scale model for compressible turbulence and scalar transport, *Phys. Fluids* A 3, Vol. 11, pp. 2746-2757.

Morris, W.D. (1981) *Heat transfer and fluid flow in rotating coolant channels*, Research Studies Press.

Murata, A. and Mochizuki, S. (2000) Large eddy simulation with a dynamic subgrid-scale model of turbulent heat transfer in an orthogonally rotating rectangular duct with transverse rib turbulators, *Int. J. Heat Mass Transfer*, Vol. 43, pp. 1243-1259.

Murata, A. and Mochizuki, S. (2001) Effect of centrifugal buoyancy on turbulent heat transfer in an orthogonally rotating square duct with transverse or angled rib turbulators, *Int. J. Heat Mass Transfer*, Vol. 44, pp. 2739-2750.

Patankar, S.V., Liu, C.H. and Sparrow, E.M. (1977) Fully developed flow and heat transfer in ducts having streamwise-periodic variations of cross-sectional area, *J. Heat Transfer*, Vol. 99, pp. 180-186.

Vreman, B., Guerts, B. and Kuerten, H. (1994), On the formulation of the dynamic mixed subgrid scale model, *Phys. Fluids*, Vol. 6, pp. 4057-4059.

Wagner, J.H., Johnson, B.V., Graziani, R.A. and Yeh, F.C. (1992) Heat transfer in rotating serpentine passages with trips normal to the flow, *J. Turbomachinery*, Vol. 114, pp. 847-857.

Wang, G. and Vanka, S.P. (1995) Convective heat transfer in periodic wavy passages, *Int. J. Heat Mass Transfer*, Vol. 38, pp. 3219-3230.